Published in final edited form as:
Invest Ophthalmol Vis Sci. 2008 July ; 49(7): 2985–2992. doi:10.1167/iovs.07-1651.

A Primate Model of Nonarteritic Anterior Ischemic Optic Neuropathy

Celia S. Chen[1,2,3,4], **Mary A. Johnson**[4,5], **Robert A. Flower**[5], **Bernard J. Slater**[5], **Neil R. Miller**[1,2,3], and **Steven L. Bernstein**[5,6,7]

[1]Department of Ophthalmology, The Johns Hopkins University School of Medicine, Baltimore, Maryland [2]Department of Neurology, The Johns Hopkins University School of Medicine, Baltimore, Maryland [3]Department of Neurosurgery, The Johns Hopkins University School of Medicine, Baltimore, Maryland [5]Department of Ophthalmology and Visual Science, University of Maryland School of Medicine, Baltimore, Maryland [6]Department of Anatomy and Neurobiology, University of Maryland School of Medicine, Baltimore, Maryland [7]Department of Genetics, University of Maryland School of Medicine, Baltimore, Maryland.

Abstract

PURPOSE—Nonarteritic anterior ischemic optic neuropathy (NAION) is an optic nerve (ON) stroke and a leading cause of sudden ON-related vision loss. A primate (p)NAION model is crucial to further understanding of the clinical disorder and can provide information regarding the pathophysiology of other central nervous system (CNS) ischemic axonopathies. In the current study, a primate model of NAION was developed, and short-and long-term responses to this condition were characterized.

METHODS—pNAION was induced with a novel photoembolic mechanism. Short- and long-term responses were evaluated by minimally invasive testing (electrophysiology, fundus photography, indocyanine green and fluorescein angiography, and magnetic resonance imaging) and compared with histologic and immunohistochemical findings.

RESULTS—Optic disc edema, similar to that observed in cases of human NAION was seen 1 day after induction, with subsequent resolution associated with the development of optic disc pallor. Magnetic resonance imaging (MRI) performed 3 months after induction revealed changes consistent with ON atrophy. Electrophysiological studies and vascular imaging suggest an ON-limited infarct with subsequent axonal degeneration and selective neuronal loss similar to that seen in human NAION. ON inflammation was evident 2 months after induction at the site of the lesion and at distant sites, suggesting that inflammation-associated axonal remodeling continues for an extended period after ON infarct.

CONCLUSIONS—pNAION resembles human NAION in many respects, with optic disc edema followed by loss of cells in the retinal ganglion cell (RGC) layer and ON remodeling. This model should be useful for evaluating neuroprotective and other treatment strategies for human NAION as well as for other ischemic processes that primarily affect CNS white-matter tracts.

Corresponding author: Steven L. Bernstein, Department of Ophthalmology, University of Maryland, School of Medicine, 10 S. Pine Street, Baltimore, MD 21201; slbernst@umaryland.edu.

[4]Contributed equally to the work and therefore should be considered equivalent authors.

Disclosure: **C.S. Chen**, None; **M.A. Johnson**, None; **R.A. Flower**, None; **B.J. Slater**, None; **N.R. Miller**, None; **S.L. Bernstein**, None

The optic nerve (ON) is a central nervous system (CNS) tract composed of retinal ganglion cell (RGC) axons that synapse in the lateral geniculate nuclei. Nonarteritic anterior ischemic optic neuropathy (NAION) is an isolated infarct of the anterior ON.[1] Although incidence figures are not available for most countries, the incidence of NAION in the United States is 3 to 10 per 100,000 per year[2,3] and 6 per 100,000 per year in mainland China.[4] No effective clinical treatments exist, largely because little is known about its pathophysiology, and there are few histopathologic studies of the acute[5] or chronic[6] condition.

Previous models of nonhuman primate ON stroke have been produced by surgical ablation of major arteries supplying the ON and posterior portions of the globe,[7] generating a model that more closely approximates arteritic anterior ischemic optic neuropathy (AAION), in part because ablation of these vessels also causes retinal and choroidal infarction. The AAION model thus is physiologically and therapeutically distinct from NAION. We have established a rodent model of NAION (rAION),[8,9] using a novel thromboembolic mechanism to affect preferentially the small vessels on the optic disc. Considerable structural and physiological differences exist between rodent and primate ON, however. First, the primate ON is highly structured, possessing a distinct, well-formed barrier within the anterior ON, the lamina cribrosa, which in rodents is present but extremely attenuated. Second, the rodent ON vascular circulation is distinct from that of primates. Third, the rodent immune response is considerably different from that of primates. Fourth, there are significant differences in the time-associated responses to CNS infarcts in primates and rodents. Fifth, the primate retina contains a highly specialized retinal region, the macula, with a high density of RGCs.[10–12] These biological differences between the two mammalian families make it difficult to identify accurately the clinically relevant targets for treatment and to predict treatment responses and timing for NAION in humans and for human white-matter infarcts in general.

Although ex vivo isolated ON preparations are used to study white-matter ischemia[13–15] and to evaluate CNS axon regeneration,[16] such preparations cannot be used to analyze effectively the long-term effects such as ischemia-associated inflammation.[17] Thus, we generated a nonhuman primate model that clinically, electrophysiologically, and angiographically closely resembles human NAION (pNAION) so that we could characterize the various ON-associated mechanistic, cellular, and immune-related changes associated with this condition in living primates.

METHODS

Animal protocols were approved by the appropriate Institutional Animal Care and Utilization Committee (IACUC) and adhered to the ARVO Statement for the Use of Animals in Ophthalmic and Vision Research. Male rhesus monkeys (*Maccaca mulatta*; age, 4–6 years; weight, 6–10 kg) were initially anesthetized with ketamine 10 mg/xylazine 2 mg/kg, intubated, and supported with inhaled isoflurane, oxygen, and nitrous oxide mixture.

Rose Bengal (RB) Toxicology

Toxicological studies of RB were performed before pNAION induction experiments. Rose Bengal (2,4,5,7-tetra-iodo-3′,4′,5′,6′-tetrachlorofluorescein, 90% purity; Sigma-Aldrich, St. Louis, MO; 5 mg/mL) was administered intravenously through the saphenous vein in a dose of 2.5 mg/kg. Animals were examined clinically at days 1 and 3 and then weekly up to 8 weeks for potential RB-induced toxicity. Blood obtained by venipuncture was used to assess systemic biochemical, hepatic, and hematologic responses to the dye.

pNAION Induction

The intraocular portion of the ON (the optic disc) was visualized with a Glasser monkey contact lens (Ocular Instruments, Inc., Bellevue, WA), and pNAION was induced by injecting RB dye intravenously in a dose of 2.5 mg/kg. RB was intravascularly photoactivated in the optic disc with a neodymium-Yttrium aluminum garnet (Nd:YAG), frequency-doubled diode laser (532 nm) with a 1.06-mm spot size, at 200 mW, for times ranging from 7 to 10 seconds. For sham treatment, an identical laser light illumination and power were used without RB dye.

ON Vascular Imaging

Clinical ON vascular imaging was performed by using both fluorescein angiography (FA) and indocyanine green angiography (ICGA). FA was performed at 1 day and then at 1, 2, 4, 6, 8, and 12 weeks after pNAION induction, by intravenously injecting 0.25 mL of fluorescein dye 25% (AK-Fluor; AMP; Akorn, Decatur, IL). Photographs were obtained with a fundus camera (Topcon, Tokyo, Japan) equipped with a standard exciter filter transmitting blue-green light at 465 to 490 nm, the peak excitation range of fluorescein, and a barrier filter transmitting a narrow band of yellow at fluorescein's peak emission range of 520 to 530 nm. High-resolution, high-speed pulsed-laser ICGA was performed with a fundus camera (Carl Zeiss Meditec, Inc., Oberkochen, Germany) modified to illuminate the fundus with 805-nm diode laser light and to record images using a 680 × 520 pixel charge-coupled device (CCD; Visics Corp, Wellesley, MA), in front of which was placed a band-pass filter having a peak transmission corresponding to the 830-nm emission of ICG dye. A commercial software platform was used for image recording and analysis (Interactive Data Language [IDL]; Research Systems, Inc., Boulder, CO).

Electrophysiology

Before all recordings, the monkey's pupils were dilated with topical 1.0% cyclopentolate, 2.5% phenylephrine, and 1.0% tropicamide. ON function was evaluated with visual evoked potentials (VEPs), RGC function with pattern-evoked ERGs (PERGs), and retinal function with standard Ganzfeld flash ERGs.

Pattern ERG and VEP—Simultaneous pERG and VEP recordings were obtained with the monkey in the prone position, and a Burian-Allen bipolar contact lens electrode was placed on the eye. Potentials were recorded from each eye separately. To record simultaneous VEP and PERG waveforms, we altered a fundus camera (Topcon) by inserting a 2-cm screen from a head-mounted display into the split viewer pathway. The input to the screen was an alternating (1.9 Hz) black-and-white checkerboard pattern having a luminance of 109 cd/m^2 at a contrast of 86% and generated by the electrophysiology-recording unit (UTAS 2000; LKC Technologies, Inc., Gaithersburg, MD). The location of the screen was adjusted so that it was conjugate to the plane of the tested pupil. In this way, when the monkey's retina was in focus, the image of the checkerboard was in focus on the monkey's retina. The field size stimulated was 46°. The array of check sizes varied in logarithmic steps from 23 minutes to 5.75°.

For VEP recordings, the active electrode (Oz) was placed above the inion in the midline over the shaved skull, the reference electrode was placed in the midline frontal position (Fz), and the ground electrode was placed in the left arm. Recordings for all check sizes were repeated at least twice per eye. For the analysis of PERGs, the latencies and amplitudes of P50 (time from trough-to-peak amplitude) and N95 (time from the peak P50 to trough of the electrical response) waves were used.[18] The untreated eye of each monkey was used for internal comparison (control).

Flash ERG—Flash ERGs were performed after 30 minutes of dark adaptation. A Burian-Allen bipolar electrode was placed in each eye and the ground electrode placed on the vertex.

Responses were elicited according to the ISCEV (International Society for Clinical Electrophysiology of Vision) protocol.[19] High and low band-pass filters were set at 0.3 and 500 Hz, respectively. Oscillatory potentials were recorded under the same circumstances but with band-pass filters set to 100 to 500 Hz.

Magnetic Resonance Imaging (MRI)

High-resolution MRI was performed on a 3.0-T scanner (Signa; GE Medical Systems, Milwaukee, WI) with a standard coil on the monkey induced with 7 seconds of exposure. MRI was performed at 12 weeks after pNAION induction in the right eye, and differences between the pNAION and control eye were compared. The scanning protocol consisted of 1.0-mm thin sections using both T_2-weighted and fat-suppressed, noncontrast T_1-weighted images. Magnified views of the ON were reobtained in selected sections in 0.7-mm thin slices.

Tissue Preparation

The animals were euthanatized for histologic analyses at various times after pNAION or sham induction while under deep pentobarbital anesthesia. They were exsanguinated immediately after euthanatization by intracardiac perfusion with normal saline with 50 U/mL sodium heparin, followed by 2.0 L of 4% paraformaldehyde and phosphate-buffered saline (PF-PBS).

The eyes were harvested with at least 5 mm of intact ON. The globes were opened tangentially at the limbus and bisected horizontally through the macula and vertically, with the ON as a central reference point, separating them into superior, inferior, temporal, and nasal retinal quadrants. Each quadrant was then further bisected to generate two equal portions for histology or other analyses.

Retinal tissue used for histology was post-fixed in PF-PBS, paraffin embedded, and sectioned at 7 μm. Sections of ON from each eye were removed and fixed for both light and electron microscopy with either PF-PBS or paraformaldehyde-glutaraldehyde (4-FIG). Tissues used for electron microscopy were fixed with osmium and uranyl acetate.

Histologic Analysis

Retinal cell layers were analyzed, and loss of cells in the ganglion cell layer (GCL) were quantified in the macula and the superior retinal quadrants by using hematoxylin and eosin (H&E)–stained step-cut sections. Differences in the number of cells between the control and pNAION eyes were analyzed with a nonpaired, nonparametric two-tailed Student's *t*-test (Stata statistical software; ver. 9.0; StataCorp, College Station, TX).

ONs were cut in cross section at 0.5-μm intervals, stained with toluidine blue, and examined at 650× magnification. PF-fixed retina–ON junctions were embedded in paraffin and sectioned at 7-μm intervals. Paraffin-embedded sections were either stained with H&E or reacted with primary rabbit antibody to IBA-1 (Wako Pure Chemicals, Osaka, Japan), which recognizes the ionized calcium-binding receptor membrane protein specifically expressed in inflammatory cells (i.e., macrophages and microglia),[20] APC-1 (an oligodendrocyte and astrocyte nuclei marker), and glial acidic fibrillary protein (GFAP), which identifies astrocytes and glial scarring. After primary antibody labeling, sections were reacted with the appropriate fluorescent-labeled donkey secondary antibodies (Jackson ImmunoResearch, West Grove, PA), DAPI (4′,6′-diamino-2-phenylindole) counterstained, and examined with confocal microscopy.

RESULTS

RB Toxicity

RB injected intravenously at a dose of 2.5 mg/kg was not associated with evidence of biological toxicity in any of the animals (Table 1). Specifically, liver enzymes showed no consistent or significant alterations after treatment, nor were any significant alterations seen in serum electrolytes or hematologic parameters. No changes in the appearance of the ONs or retinas were detected in the control eyes of the animals, nor were there any abnormalities detected in the eyes with any electrophysiological tests (i.e., visual evoked potentials [VEP], pattern [P] ERG, Ganzfeld ERG; Fig. 3, Baseline).

Clinical Responses to pNAION Induction

The optic disc was normal before induction of pNAION in all animals (Fig. 1A). Within 1 day after induction, optic disc edema was present and was associated with peripapillary optic disc hemorrhages (Fig. 1B). The edema and hemorrhages were still present 7 days after induction (Fig. 1C) but had generally resolved by 14 days (Fig. 1D). Disc edema was replaced by sectoral optic disc pallor at 70 days after induction (Fig. 1E).

Angiographic Findings

Disruption of the blood– brain barrier (BBB) after pNAION induction was demonstrated by leakage of fluorescein dye from optic disc vessels within 1 day after induction (Fig. 2B), a phenomenon not observed in preinduction ONs (Fig. 2A). The leakage was prominent 7 to 14 days after pNAION induction (Fig. 2C), with resolution by 4 weeks, at which time there was disc staining only (Fig. 2D). High-speed, high-resolution ICGA showed normal filling of the intraretinal and choroidal vasculature before induction (Fig. 2E) as well as throughout the period of observation (Figs. 2F–H), although in some animals, transient reduction in venous outflow was observed within the first 48 hours after induction and then resolved.

Electrophysiology

Seven-second pNAION-induced eyes had normal amplitudes and latencies before induction but subsequently showed a 50% to 60% reduction in VEP amplitude at 1 week compared with that in control eyes (Fig. 3, top). The pNAION eyes continued to show relatively constant, reduced VEP amplitudes throughout the observation period, whereas control eyes had VEP amplitudes similar to baseline values. The latencies of the P100 peaks remained normal in both control and pNAION eyes throughout. PERG amplitudes were normal and comparable in the two eyes before induction (Fig. 3, lower panel). Shortly after induction, however, N95 amplitudes in pNAION eyes became reduced, whereas N95 amplitudes in control eyes remained normal. The reduction in N95 amplitude was maintained over the entire period of assessment. P50 amplitudes were also slightly reduced in the treated eye during this period. In contrast to the VEP and PERG amplitudes, flash ERGs remained normal in both control and pNAION-induced eyes during the entire period of assessment (Fig. 4).

Magnetic Resonance Imaging

MRI revealed findings consistent with atrophy of the ON from a pNAION-induced eye 12 weeks after induction compared with the animal's control fellow eye. These changes consisted of an increased fluid signal surrounding the ON in T_2-weighted images and a reduced diameter of the ON shadow with a surrounding increased fluid signal in T_1-weighted images. Evidence ON atrophy was present throughout the length of the ON from the globe to the optic chiasm.

Histopathology

The retinas of pNAION-induced eyes ≥84 days after induction revealed changes consistent with isolated loss of cells and their axons. These consisted of thinning of the nerve fiber layer (NFL) and reduced numbers of cells in the GCL in retinal sections from pNAION-induced eyes, compared with corresponding sections from control eyes (compare Fig. 5A with Fig. 5F). There also was a quantitative loss of cells in the GCL in pNAION-induced eyes. For example, mean GCL cell numbers were 93 ± 19.4 in the macula of the control eye versus 33.3 ± 10.1 cells in the same region of a 10-second–induced pNAION eye ($P = 0.002$; two-tailed *t*-test). Other retinal layers were unaffected with respect to overall structure and relative cell numbers. No statistically significant changes were seen in the number of layers of nuclei in the internuclear layer (INL: 5.22 ± 0.81 nuclear layers in control eyes versus 6.42 ± 0.83 pNAION-induced eyes) or the outer nuclear layer (ONL: 6.40 ± 0.81 nuclear layers in control eyes versus 8.3 ± 1.6 pNAION eyes; compare INL and ONL in Figs. 5A and 5F).

Compared with control eyes, pNAION-induced eyes revealed axonal disruption and increased cellularity of the ONs (compare Figs. 5C–E and 5H–J) and increased cellularity and loss of architecture in the region of the lamina cribrosa (compare Figs. 5B and 5G). Toluidine blue staining and transmission electron microscopy confirmed extensive axonal destruction in the region of the ischemic damage (Fig. 6).

The increased ON and peripapillary cellularity in pNAION-induced eyes (compare Figs. 7A and 7D) was identified as an inflammatory infiltrate that was demonstrable by IBA-1 immunostaining (Fig. 7E). As noted earlier, IBA-1 recognizes the ionized calcium-binding receptor membrane protein specifically expressed in inflammatory cells.[20] Nuclei in control ONs in the laminar and immediately retrolaminar regions were largely IBA-1 negative (Fig. 7B), whereas IBA-1 immunostained cells were consistently present in qualitatively increased numbers, not only in the laminar and immediately retrolaminar regions of pNAION-induced ONs (Fig. 7E) but also in pNAION-induced ONs at least 1 cm posterior to the lamina cribrosa, well posterior to the ischemic region (compare Figs. 7C and 7F).

DISCUSSION

The pNAION model of ON damage resembled human NAION clinically, angiographically, electrophysiologically, and histologically. pNAION-induced ON edema occurred within 1 day after induction and resolved over 2 to 3 weeks. The edema was visible as optic disc swelling and was similar to the edema in human NAION, as were the peripapillary retinal hemorrhages that appeared at about the same time.[21] This clinical picture is consistent with an ischemia-reperfusion type of CNS injury.[22,23] The edema and hemorrhages then increased over a short period after induction, suggesting that ON edema compresses initially unaffected axons and their vascular supply, resulting in secondary axonal dysfunction and extension of the primary defect. If this mechanism is responsible for progressive worsening of visual function in human NAION, control of ON edema at an early stage of the human condition may prevent or even reverse visual loss.

Optic disc pallor developed as edema resolved, again similar to the clinical findings in human NAION. In human NAION, however, these changes usually occur over 6 to 8 weeks.[24] This difference in the time of resolution of disc swelling and the development of disc pallor is consistent with the difference in lifespan between human and nonhuman primates. These data suggest that physiological mechanisms regulating edema resolution are roughly two times faster in old world, nonhuman primates than in humans.

As is the case with the clinical picture, vascular imaging in our pNAION model revealed changes that are similar to those observed in human NAION. For example, FA of eyes with

early pNAION has revealed dye leakage from the optic disc vessels, consistent with that seen in human NAION.[25] This leakage corresponds to breakdown of the BBB, a phenomenon that is one of the earliest consequences of inflammation and may itself induce further ON edema. The leakage resolves over 2 weeks, suggesting that a prolonged period is required for re-establishment of the BBB after an axonal white-matter stroke.

In contrast to the leakage of fluorescein dye from the vessels of the optic disc that was seen early in the course of pNAION followed by staining of the disc later in the course, high-resolution vascular imaging using high-speed ICGA in pNAION eyes revealed only early compromised capillary filling near the ON surface, compared with control ONs. No change in filling occurred in the adjacent retina or underlying choroid, indicating that the damage we produced in our model was restricted to the ON and did not affect the peripapillary retina or choroid.

pNAION is a primary optic neuropathy with axonal loss and secondary neuron (RGC) loss, a feature of many different optic neuropathies.[26] The retina of eyes with pNAION showed a reduction in the thickness of the nerve fiber layer as well as significant loss of RGCs that was particularly marked in the macula. These features were confirmed by electrophysiologic analysis, which revealed that pNAION primarily affected the ON axons, followed by secondary RGC degeneration. VEP amplitudes, a measure of ON axonal function, were reduced 1 day after pNAION induction compared with control eyes, and remained reduced thereafter, although VEP latencies remained normal throughout the observation period. These findings are similar to the VEP results reported in human NAION.[27] The PERG—a measure of RGC function—became abnormal soon after pNAION induction, indicating a rapid response of the RGCs to damage to their axons. The function of the rest of the retina remained normal, however, as the flash ERG remained unchanged after induction. The preservation of flash ERG response is similar to that in clinical NAION.[27]

MRI is often used to evaluate the extent and progression of CNS infarcts.[28] In one animal that was subsequently shown to have a 60% loss of GCL cells, MRI performed 80 days after pNAION induction revealed changes consistent with isolated ON atrophy. Thus, as might be expected, pNAION, like human NAION, induced long-term postinfarct white-matter atrophy along the entire length of the axon, again consistent with both electrophysiologic and histologic data.

A potentially important finding in our pNAION model is evidence of ON inflammation detected by the immunohistochemical marker IBA-1. Not only were there a significant number of inflammatory cells in the region of the ON infarct, but ON regions >1 cm distal to the primary lesion also contained a qualitatively increased number of inflammatory cells compared with control ONs. These findings are similar to those in other models of white-matter ischemia and suggest that, at least in our pNAION model, ON ischemia results in early recruitment of macrophages to the ischemic infarct core. Although the initiating insult is different in pNAION than in human NAION, the ophthalmoscopic appearance, electrophysiologic findings, and angiographic findings are identical with those in human NAION, and the infarct location is histologically similar to the few reported cases of human NAION,[5,6] thus suggesting not only that pNAION is an appropriate model for human NAION but also that our finding of an inflammatory response within the ON shortly after production of ON ischemia may be applicable to the human condition. Such postischemia inflammation, with macrophage infiltration into the ON, could have two opposing roles. On the one hand, the inflammation can cause increased tissue destruction, edema, and compression of adjacent vessels and axons, resulting in further loss of visual sensory function and decreasing the likelihood of significant visual recovery.[1,21] On the other hand, macrophages play a major role in phagocytosis and removal of myelin debris after ischemic axonal degeneration, enhancing the potential for

remyelination[29] and paving the way for subsequent axon regeneration.[30] Microglia also may produce trophic factors that afford neuroprotection by recruiting macrophages into the ischemic area.[31] Thus, after ON ischemia, several types of inflammatory processes occur that work at cross purposes. By selectively manipulating this inflammatory response, it may be possible to develop new treatment modalities for NAION and other ischemic ON diseases.

In summary, we have generated the first reproducible, nonhuman primate model of NAION. We have characterized the functional and histologic changes that occur after induction. The model is clinically, angiographically, electrophysiologically, and histopathologically similar to human NAION. We have also shown that that, similar to other CNS regional infarcts, post-ON infarct inflammation occurs within the nerve and in the laminar region. The similarity of nonhuman, old world primates to humans suggests that the pNAION model can be used to provide greater understanding of the human mechanisms of axonal and neural interaction after axonal ischemia and may be useful in the development of neuroprotective strategies essential for understanding the effects of putative treatments aimed at ameliorating damage from human NAION and other white-matter strokes.

Acknowledgements

The authors thank Rao Gullipalli for his expertise in MRI design and study, and Ned Kriel and Turhan Coksayan and Theresa Alexander for veterinary support.

Supported by the American Australian Association Education Fellowship (CSC), the Donegan Fund for Anterior Ischemic Optic Neuropathy Research (CSC, MAJ, NRM, SLB), an unrestricted grant from Research to Prevent Blindness to the University of Maryland (SLB), and National Eye Institute Grant R01-EY015304-01 (SLB).

References

1. Arnold AC. Pathogenesis of nonarteritic anterior ischemic optic neuropathy. J Neuroophthalmol 2003;23(2):157–163. [PubMed: 12782932]
2. Johnson LN, Arnold AC. Incidence of nonarteritic and arteritic anterior ischemic optic neuropathy: population-based study in the state of Missouri and Los Angeles County, California. J Neuroophthalmol 1994;14(1):38–44. [PubMed: 8032479]
3. Hattenhauer MG, Leavitt JA, Hodge DO, Grill R, Gray DT. Incidence of nonarteritic anterior ischemic optic neuropathy. Am J Ophthalmol 1997;123(1):103–107. [PubMed: 9186104]
4. Xu L, Wang Y, Jonas JB. Incidence of nonarteritic anterior ischemic optic neuropathy in adult Chinese: the Beijing Eye Study. Eur J Ophthalmol 2007;17(3):459–460. [PubMed: 17534837]
5. Tesser RA, Niendorf ER, Levin LA. The morphology of an infarct in nonarteritic anterior ischemic optic neuropathy. Ophthalmology 2003;110(10):2031–2035. [PubMed: 14522783]
6. Knox DL, Kerrison JB, Green WR. Histopathologic studies of ischemic optic neuropathy. Trans Am Ophthalmol Soc 2000;98:203–202. [PubMed: 11190024]
7. Hayreh SS. Anterior Ischemic optic neuropathy. I. Terminology and pathogenesis. Br J Ophthalmol 1974;58:955–963. [PubMed: 4376415]
8. Bernstein SL, Guo Y, Kelman SE, Flower RW, Johnson MA. Functional and cellular responses in a novel rodent model of anterior ischemic optic neuropathy. Invest Ophthalmol Vis Sci 2003;44(10): 4153–4162. [PubMed: 14507856]
9. Goldenberg-Cohen N, Guo Y, Margolis FL, Miller NR, Cohen Y, Bernstein SL. Oligodendrocyte dysfunction following induction of experimental anterior optic nerve ischemia. Invest Ophthalmol Vis Sci 2005;46:2716–2725. [PubMed: 16043843]
10. May CA, Lütjen-Drecoll E. Morphology of the murine optic nerve. Invest Ophthalmol Vis Sci 2002;43 (7):2206–2212. [PubMed: 12091418]
11. Morrison JC, Johnson EC, Cepurna WO, Funk RH. Microvasculature of the rat optic nerve head. Invest Ophthalmol Vis Sci 1999 Jul;40(8):1702–1709. [PubMed: 10393039]

12. Davis WC, Hamilton MJ. Comparison of the unique characteristics of the immune system in different species of mammals. Vet Immunol Immunopathol 1998;63(1–2):7–3. [PubMed: 9656435]
13. Meakin PJ, Fowler MJ, Rathbone AJ, et al. Fructose metabolism in the adult mouse optic nerve, a central white matter tract. J Cereb Blood Flow Metab 2007;27:86–99. [PubMed: 16670697]
14. Garthwaite G, Brown GC, Batchelor AM, Goodwin DA, Garthwaite J. Mechanisms of ischaemic damage to central white matter axons: a quantitative histological analysis using rat optic nerve. Neuroscience 1999;94:1219–1230. [PubMed: 10625062]
15. Stys, PK.; Ransom, BR.; Black, JA.; Waxman, SG. Anoxic/ischemic injury in axons. In: Waxman, SG.; Kocsis, JD.; Stys, PK., editors. The Axon. New York: Oxford University Press; 1995. p. 462-479.
16. Isenmann S, Kretz A, Cellerino A. Molecular determinants of retinal ganglion cell development, survival, and regeneration. Prog Retin Eye Res 2003;22(4):483–543. [PubMed: 12742393]
17. Pantoni L. Experimental approaches to white matter disease. Dement Geriatr Cogn Disord 1998;9:20–24. [PubMed: 9716240]
18. Bach M, Hawlina M, Holder GE, et al. Standard for pattern electroretinography: International Society for Clinical Electrophysiology of Vision. Doc Ophthalmol 2000;101:11–18. [PubMed: 11128964]
19. Marmor MF, Holder GE, Seeliger MW, Yamamoto S. Standard for clinical electroretinography. Doc Ophthalmol 2004;108:107–114. [PubMed: 15455793]
20. Ito D, Tanaka K, Suzuki S, Dembo T, Fukuuchi Y. Enhanced expression of Iba1, ionized calcium-binding adapter molecule 1, after transient focal cerebral ischemia in rat brain. Stroke 2001;32(5): 1208–1215. [PubMed: 11340235]
21. Beck RW, Servais GE, Hayreh SS. Anterior ischemic optic neuropathy IX: cup to disk ratio and its role in pathogenesis. Ophthalmology 1987;94:1503–1510. [PubMed: 3684223]
22. Wakita H, Tomimoto H, Akiguchi I, et al. Axonal damage and demyelination in the white matter after chronic cerebral hypoperfusion in the rat. Brain Res 2002;924(1):63–70. [PubMed: 11743996]
23. Denner L. Stroke and ischemia-reperfusion injury. IDrugs 2001;4(1):20–22. [PubMed: 16034692]
24. Hayreh SS, Zimmerman MB. Optic disc edema in non-arteritic anterior ischemic optic neuropathy. Graefes Arch Clin Exp Ophthalmol 2007;245(8):1107–1121. [PubMed: 17219123]
25. Arnold AC, Badr MA, Hepler RS. Fluorescein angiography in nonischemic optic disc edema. Arch Ophthalmol 1996;114(3):293–298. [PubMed: 8600889]
26. Gupta N, Yucel YH. Glaucoma as a neurodegenerative disease. Curr Opin Ophthalmol 2007;18(2): 110–114. [PubMed: 17301611]
27. Janaky M, Fulop Z, Palffy A, Benedek K, Benedek G. Electrophysiological findings in patients with nonarteritic anterior ischemic optic neuropathy. Clin Neurophysiol 2006;117(5):1158–1166. [PubMed: 16551511]
28. Arnold AC, Hepler RS, Hamilton DR, Lufkin RB. Magnetic resonance imaging of the brain in nonarteritic ischemic optic neuropathy. J Neuroophthalmol 1995;15(3):158–160. [PubMed: 8574360]
29. Selvaraju R, Bernasconi L, Losberger C, et al. Osteopontin is upregulated during in vivo demyelination and remyelination and enhances myelin formation in vitro. Mol Cell Neurosci 2004;25 (4):707–721. [PubMed: 15080898]
30. Yin Y, Henzl MT, Lorber B, et al. Oncomodulin is a macrophage-derived signal for axon regeneration in retinal ganglion cells. Nat Neurosci 2006;9(6):843–852. [PubMed: 16699509]
31. Harada T, Harada C, Kohsaka S, et al. Microglia-Müller glia cell interactions control neurotrophic factor production during light-induced retinal degeneration. J Neurosci 2002;22:9228–9236. [PubMed: 12417648]

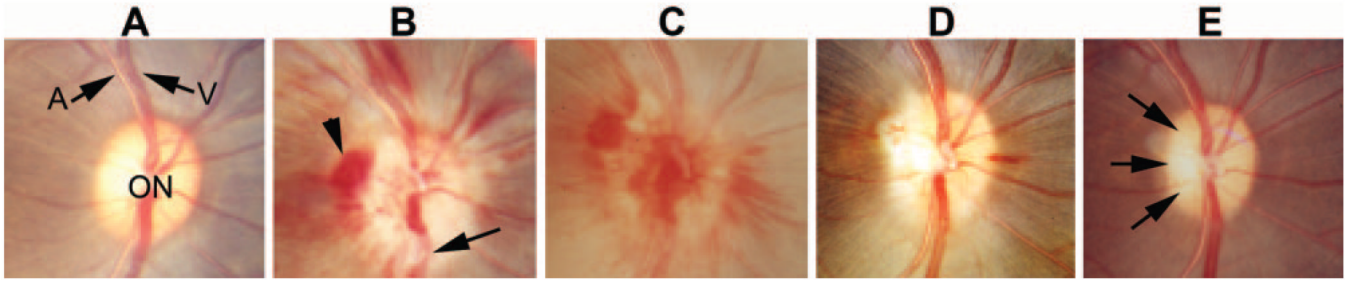

FIGURE 1.

Clinical appearance of the optic disc before and after induction of pNAION. (**A**) Before induction, the optic disc (ON) was normal in appearance, and the retinal arteries (A) and veins (V) were not obscured. Note that the disc had almost no central cup, thus mimicking a human disc at risk. (**B**) One day after induction, the disc was pale and swollen, with blurring of the retinal nerve fiber layer and obscuration of vessels as they cross the disc (*arrow*). Several peripapillary hemorrhages were present (*arrowhead*). (**C**) Seven days after induction, optic disc edema had increased, and extensive hemorrhages overlay and surrounded the disc. (**D**) Fourteen days after induction, much of the swelling had resolved, most of the hemorrhages had disappeared, and the optic disc was slightly pale. (**E**) Seventy days after induction, optic disc edema had resolved and the disc was pale, particularly temporally (*arrows*); the previously noted hemorrhages had resolved.

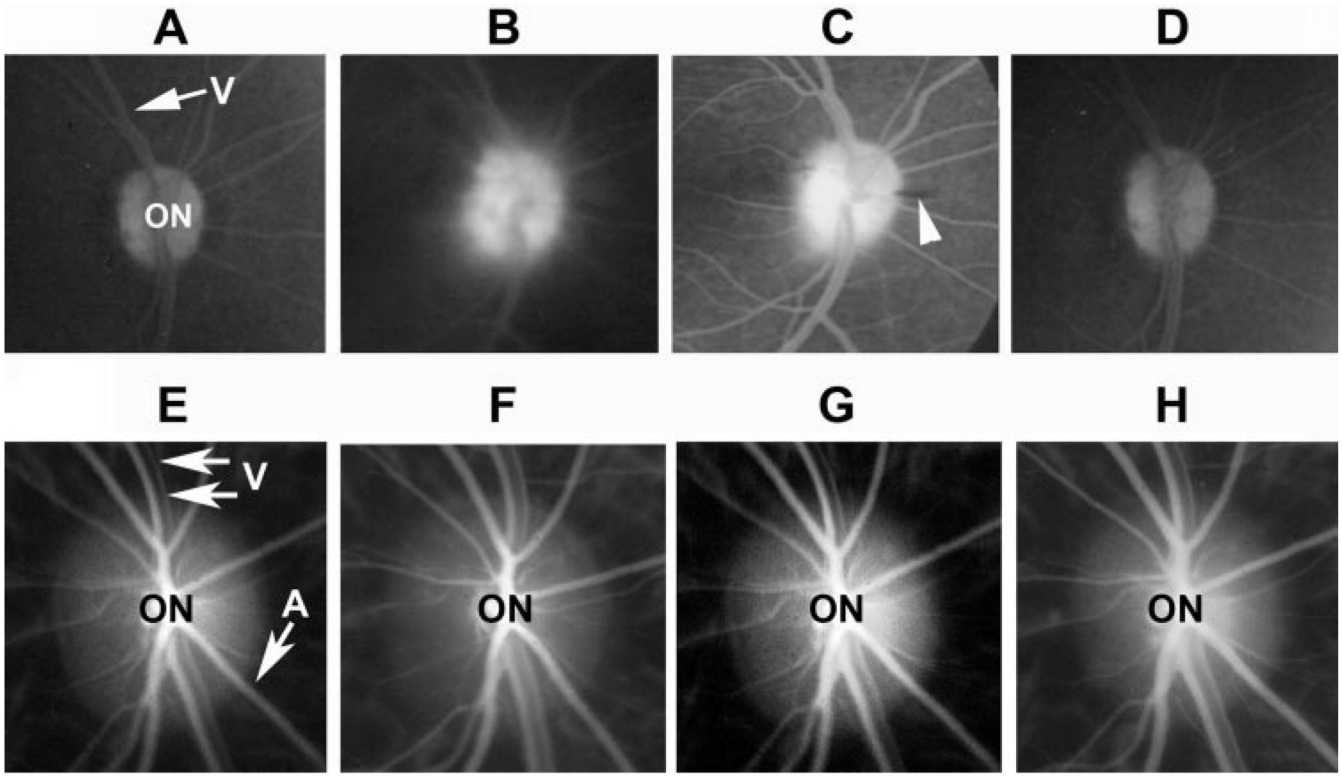

FIGURE 2.

Late arteriovenous phase FA (**A–D**) and high-resolution ICGA (**E–H**) pNAION. (**A**) Before induction, the ON margins were sharply defined; there was no dye leakage. V, retinal vein. (**B**) One day after induction, there was generalized leakage of dye from the optic disc, and the margins of the disc were obscured. (**C**) Fourteen days after induction, dye leakage persisted but was resolving. The disc margins were becoming more sharply defined. Only one peripapillary hemorrhage was present (*arrowhead*). (**D**) Twenty-eight days after induction, the margins of the disc were once again sharp. There was now diffuse disc staining but no dye leakage, suggesting re-establishment of an intact BBB. (**E**) Before induction, ICGA showed a sharply defined optic disc (ON) and laminar blood flow in the peripapillary veins (V) and arteries (A). Normal choroidal blood flow was identifiable by fine, whitish streaks. (**F**) One day after induction, no disruption of either choroidal or retinal blood flow was discernable. (**G**) Seven days after induction, choroidal and retinal blood flow remain intact. (**H**) Twenty-eight days after induction, there was no disruption of either retinal or choroidal blood flow; venous blood flow was laminar.

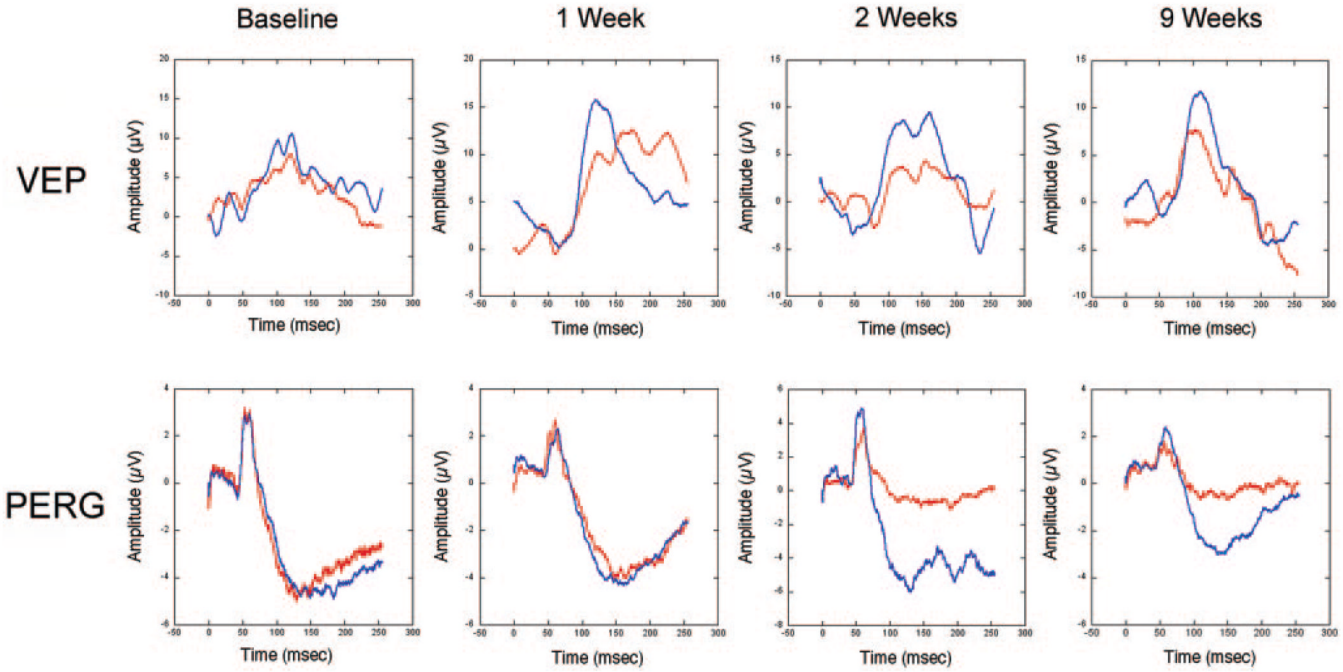

FIGURE 3.

Clinical electrophysiology of control (*blue lines*) and 7-second pNAION-induced (*red lines*) eyes. *Top*: VEP in both eyes at baseline (before induction) and at 1, 2, and 9 weeks after induction. At baseline, the VEPs were equal in the two eyes; however, at 1 week, there was a reduction in the VEP amplitude from the pNAION eye, whereas the VEP amplitude in the control eye remained normal. The reduction in VEP amplitude in the pNAION eye persisted at 2 and 9 weeks, whereas the VEP amplitude in the control eye remained normal. Note that the latency of the P100 peak remained normal in both eyes throughout the period of observation. *Bottom*: PERG of control and 7-second pNAION eyes during the same period as the VEP. At baseline, the PERG was normal in both eyes and remained normal in both eyes 1 week after induction; however, by 2 weeks after induction, there was a large reduction in the N95 PERG amplitude in the pNAION eye compared with the control eye, suggesting that intraocular RGC function declined after the ON infarct. This reduction was still present at 9 weeks. The delay in PERG reduction suggests that, at least in this animal, RGC damage did not occur immediately.

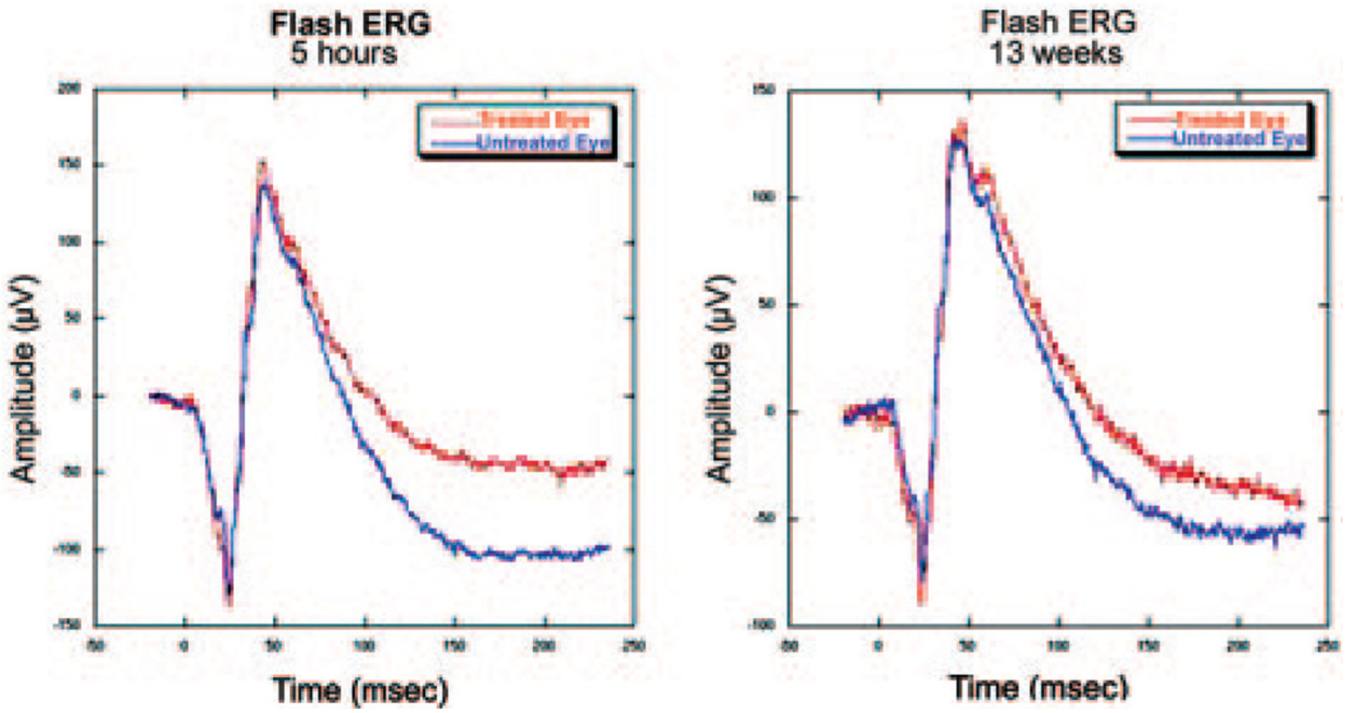

FIGURE 4.

Flash ERG potentials in control and 7-second pNAION eyes. The ERG potentials were normal and symmetric in the two eyes at 5 hours after induction and at 13 weeks after induction, indicating that general retinal function remained normal throughout the observation period.

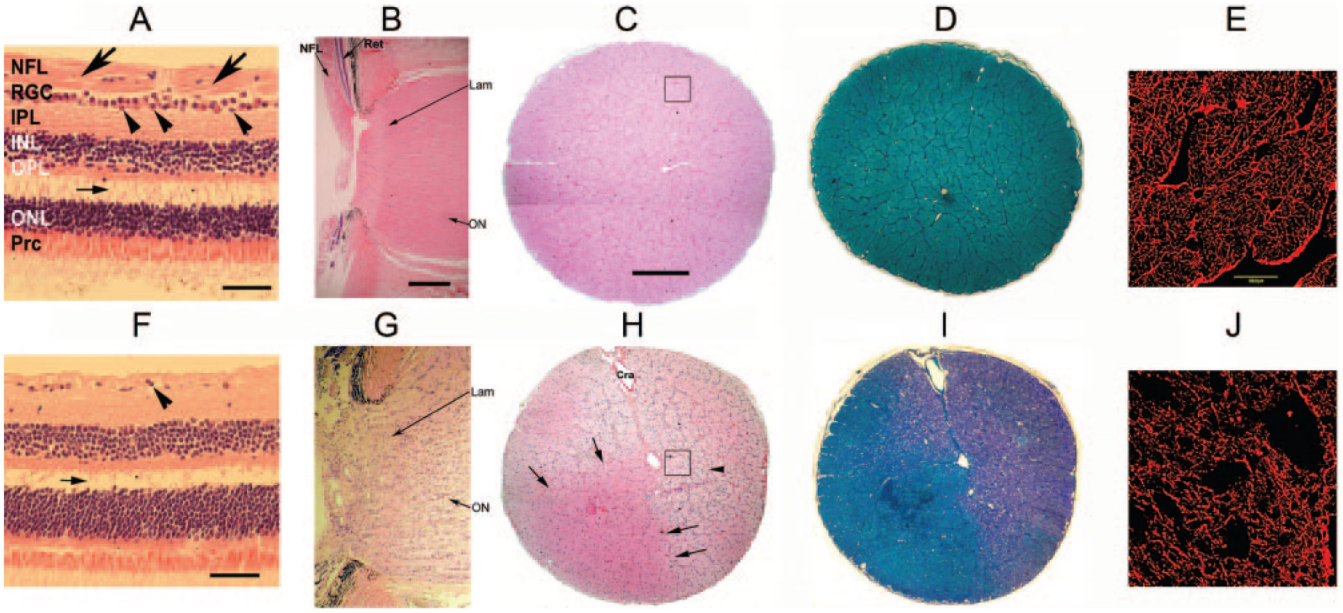

FIGURE 5.

Retinal histology in control (**A–E**) versus pNAION (**F–J**) eyes. (**A**) H&E-stained horizontal section through the macular region of the control eye shows that the retinal nerve fiber layer (NFL) was intact and of normal thickness (*arrows*), as was the RGC layer, which contained multiple layers of nuclei of RGCs and amacrine cells (*arrowheads*). There was an artifactitious separation of retinal layers between the outer plexiform layer (OPL) and the outer nuclear layer (ONL) (*small horizontal arrow*). (**B**) H&E-stained longitudinal section through the optic disc and lamina cribrosa of the control eye. The ON was normal in appearance, including the region of the lamina cribrosa (Lam). The peripapillary retinal nerve fiber layer (NFL) also appeared normal, as did the rest of the peripapillary retina (Ret). (**C**) H&E-stained cross section of the control ON. Individual axon bundles were regular in appearance with normal cellularity. *Black-outlined inset* appears at higher magnification in (**E**). (**D**) Cross section of the control ON stained with Luxol fast blue. Axons were normal in appearance and there was no evidence of demyelination. (**E**) Confocal microscopy of a cross section of the control ON from (**C**) stained for GFAP. Note intact architecture with no disruption or loss of astrocytes. (**F**) H&E-stained section through the macular region in a pNAION eye. The NFL was reduced in thickness and the RGC layer was almost nonexistent (*arrowhead*). As in (**A**), there was an artifactitious separation of retinal layers between the OPL and ONL (*small horizontal arrow*). (**G**) H&E-stained longitudinal section through the ON and peripapillary retina in the pNAION eye. There was disruption of the normal architecture of the ON, including the disc, laminar (lam), and immediate retrolaminar regions, with increased cellularity in all areas. (**H**) H&E-stained cross section of the ON in the pNAION eye. There was loss of architecture with increased cellularity (*arrowhead*) except for a wedge-shaped, unaffected quadrant that was normal in appearance (*arrows*). *Black-outlined inset* appears at higher magnification in (**J**). (**I**) Cross section of the ON from the pNAION eye stained with Luxol fast blue showing extensive demyelination. (**J**) Confocal microscopy of a cross section of the pNAION ON from (**H**) stained for GFAP. There was extensive disruption of architecture. IPL, inner plexiform layer; INL, inner nuclear layer; Prc, photoreceptors. Cra, central retinal artery. Scale bar: (**A**, **F**) 50 μm; (**B–D**, **G–I**) 500 μm.

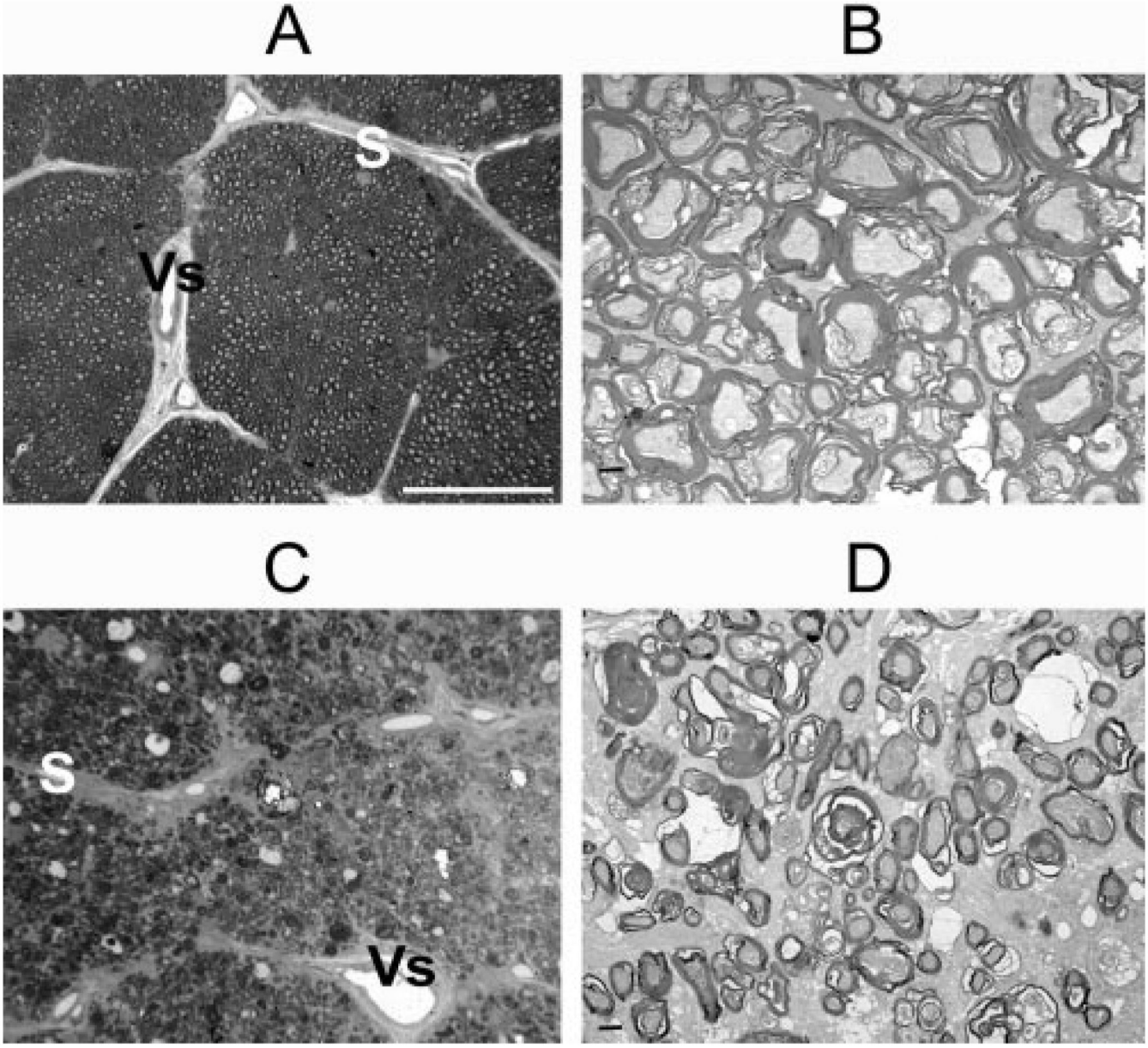

FIGURE 6.

Cross sections of ONs from normal (**A**, **B**) and pNAION (**C**, **D**) eyes. (**A**) Toluidine blue–stained section from a control ON showed normal-appearing axon bundles separated by fibrovascular pial septae (S), some of which contained capillaries (Vs). Axons were seen as small, unstained circles surrounded by stained myelin sheaths. (**B**) TEM section from same area as in (**A**) showed regular, myelinated axon bundles. (**C**) Toluidine blue–stained section from a pNAION ON showed loss of axons, reduction in size of axon bundles, and thickening and disruption of fibrovascular pial septae (S). V, central retinal vein. (**D**) TEM section from same area as (**C**) showed extensive demyelination with shrinkage and disruption of axons. Scale bars: (**A**, **C**) 40 μm; (**B**, **D**) 1 μm.

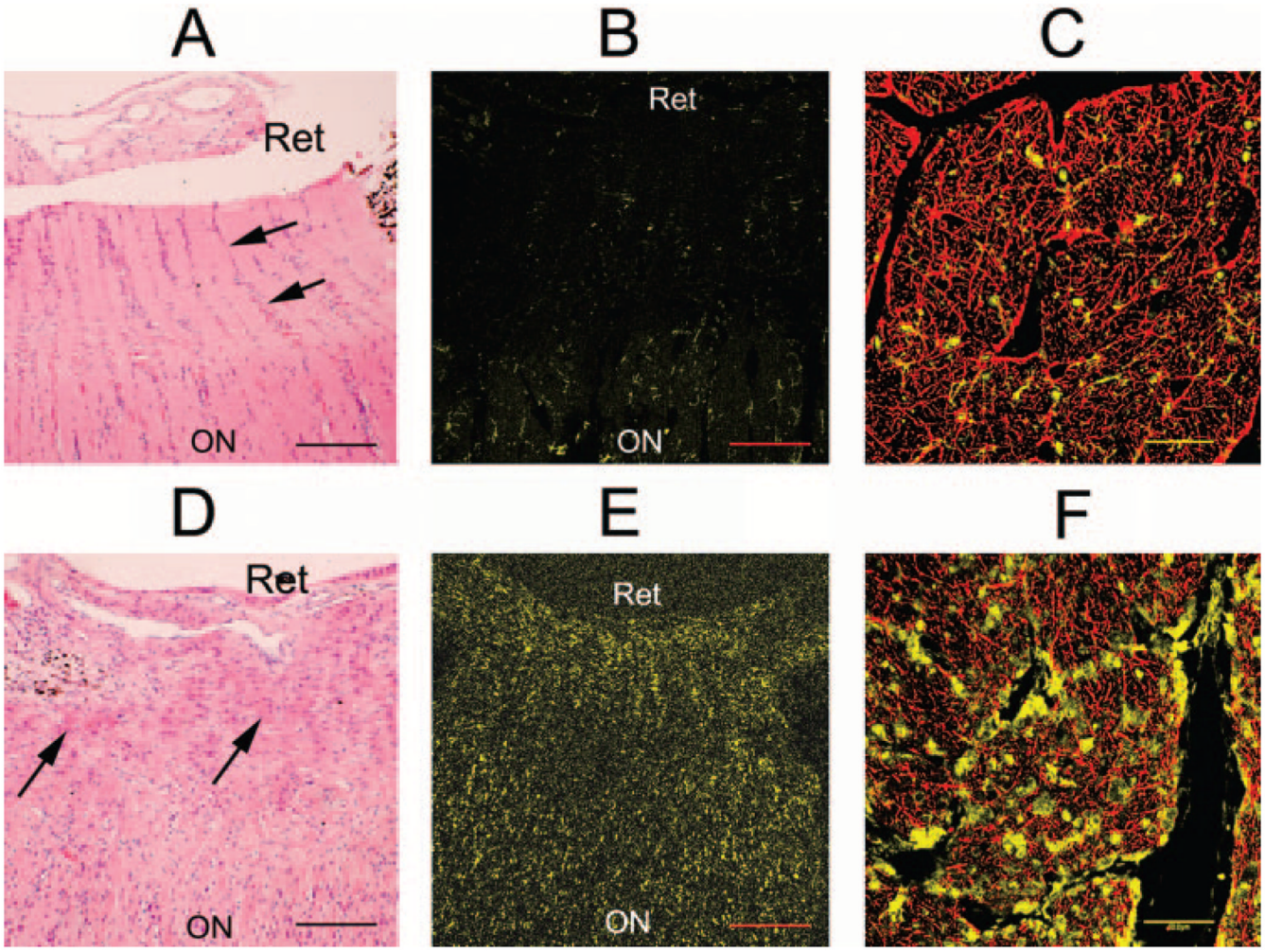

FIGURE 7.

Normal appearance of the ON of a control eye (**A–C**) versus inflammation in a nerve after induction of pNAION (**D–F**). (**A**, **B**, **D**, **E**) Longitudinal sections; (**C**, **F**) cross sections of ONs 1 cm posterior to the laminar region. (**A**) H&E-stained section of a proximal ON in a control eye. Columns of nuclei (*arrows*) were relatively evenly distributed throughout the nerve, interspersed with axonal (*light pink*) elements. (**B**) IBA-1–stained section of the same nerve showed only rare stained cells. (**C**) Confocal microscopy of a cross section of the ON from the control eye, double stained with antibodies to GFAP (*red*) and IBA-1 (*yellow*), showed a relative paucity of IBA-1–stained cell nuclei. (**D**) H&E-stained section of the proximal ON of a pNAION-induced eye. There was significant disruption of normal architecture associated with an increased number of cells and deposition of eosinophilic material (*arrows*) throughout the area. The cells are present in the prelaminar, laminar, and immediately retrolaminar regions. (**E**) IBA-1–stained section of the proximal ON from the pNAION-induced eye revealed many positively stained cells in the peripapillary region and interspersed throughout the prelaminar, laminar, and immediately retrolaminar regions (*arrowheads*). (**F**) Confocal microscopy of a cross section of the ON from the pNAION-induced eye, double-stained with antibodies for GFAP and IBA-1, ~1 cm posterior to the laminar region, well posterior to the ischemic lesion, double-stained with GFAP (*red*) and IBA-1 (*yellow*). Note numerous IBA-1–stained cell nuclei. Scale bars: (**A**, **B**, **D**, **E**) 100 μm; (**C**, **F**) 50 μm.

Invest Ophthalmol Vis Sci. Author manuscript; available in PMC 2009 September 29.

TABLE 1

Laboratory Studies of a Representative Animal after Intravenous Injection of Rose Bengal Animal Q16

	Reference Range (Male Monkey Age 3–4 y)	Baseline	Day 1	Day 4	Day 7	Day 14	Day 28
Weight (kg)		6.5	6.25	6.8	7.06	7.10	7.23
Liver function							
Total bilirubin	0.2 ± 0.1	0.2	0.3	0.3	0.2	0.2	0.2
ALP	529 ± 177	443	374	364	364	348 (L)	375
ALT	37 ± 9	36	35	30	31	22 (L)	28
AST	40 ± 13	35	60 (H)	33	32	31	45
GGT	57 ± 20	64	54	70	75	66	81 (H)
Total protein	7.3 ± 0.4	5.9	6.7	6.9	6.7 (L)	5.9 (L)	6.5 (L)
Albumin	4.6 ± 0.3	3.7	4.3	4.4	4.1 (L)	3.7 (L)	4.1 (L)
Electrolytes							
Glucose	73 ± 16	183 (H)	61	85	64	96 (H)	32 (L)
BUN	18 ± 3	22	22	21	23 (H)	28 (H)	21
Creatine	0.9 ± 0.1	0.8	0.8	0.8	0.8	0.7	1
Phosphate	5.2 ± 0.6	4.8	5.1	5.9	5	4.8	8.2 (H)
Sodium	151 ± 9	144	145	145	146	146	147
Potassium	4.7 ± 0.6	4.2	3.4 (L)	4 (L)	3.8 (L)	4.1	4.6
Chloride	105 ± 8	108	105	106	108	106	106
Magnesium		1.3	1.4	1.5	1.4	1.2	1.8
Cholesterol	138 ± 20	112 (L)	148	139	117 (L)	122	123
Triglyceride	50 ± 16	52	16 (L)	38	97 (H)	101 (H)	58
Comment			4 + hemolysis	1 + hemolysis		1 + hemolysis	
Complete blood count							
Hbg	12.9 ± 0.7	11.6	12.1		11.8	11	12.1
WBC	10.5 ± 2.8	12	5.8		7.9	8.6	6
Platelets		356	291		408	354	322

H, value higher than reference range; L, value lower than reference range.